In vivo examination of an injectable hydrogel system crosslinked by peptide-oligosaccharide interaction in immunocompetent nude mice

Tondera, C.; Wieduwild, R.; Röder, E.; Werner, C.; Zhang, Y.; Pietzsch, J.;

In vivo Examination of an Injectable Hydrogel System Crosslinked by Peptide-Oligosaccharide Interaction in Immunocompetent Nude Mice

Christoph Tondera, Robert Wieduwild, Elisabeth Röder, Carsten Werner, Yixin Zhang[*], Jens Pietzsch[*]

Christoph Tondera, Elisabeth Röder, Prof. Dr. Jens Pietzsch
Helmholtz-Zentrum Dresden-Rossendorf,
Institute of Radiopharmaceutical Cancer Research
Department of Radiopharmaceutical and Chemical Biology
Bautzner Landstraße 400
01328 Dresden, Germany
E-mail: j.pietzsch@hzdr.de

Christoph Tondera, Elisabeth Röder, Prof. Dr. Jens Pietzsch
Technische Universität Dresden, Department of Chemistry and Food Chemistry
Bergstraße 66
01062 Dresden, Germany

Dr. Robert Wieduwild, Prof. Dr. Carsten Werner, Prof. Dr. Yixin Zhang
B CUBE Center for Molecular Bioengineering, Biomolecular Interactions
Technische Universität Dresden
Arnoldstraße 18
01307 Dresden, Germany
E-mail: yixin.zhang@bcube-dresden.de

Prof. Dr. Carsten Werner
Leibniz-Institut für Polymerforschung Dresden e.V.
Max Bergmann Center of Biomaterials and Technische Universität Dresden
Hohe Straße 6
01069 Dresden, Germany

Hydrogels can serve as matrices to mimic natural tissue function and be used for wide-ranging applications such as tissue regeneration and drug delivery. Injectable hydrogels are particularly favorable because their uses are minimally invasive. However, to create mouldable substance for injection often results in compromised function and stability. Here we report an injectable hydrogel system crosslinked by peptide-oligosaccharide non-covalent interaction. The dynamic network showed fast self-healing, a property essential for injectability. Injected hydrogels in immunocompetent mice and release of encapsulated compound were monitored up to 9 months by magnetic resonance imaging (MRI) and optical imaging. This surprisingly stable hydrogel did not cause adverse inflammatory response, as analyzed by measuring cytokine levels, immunohistochemistry, and MRI. Hydrogel degradation is associated with invasion of macrophages and vascular formation. The facile synthesis, high biocompatibility and stability of this injectable hydrogel could lead to various experimental and clinical applications in regenerative medicine and drug delivery.

1. Introduction

To shift network chemistry from a covalent to a non-covalent base will allow us to develop novel materials which possess functions and properties impossible to obtain with traditional polymer linkages.[1,2] For example, to use biomaterials for tissue engineering, regenerative medicine, or drug release, an injectable hydrogel system has the advantage to substitute surgical procedures by minimally-invasive injection.[3,4] However, to develop such mouldable hydrogels fulfilling both physicomechanical prerequisites for injection and demands for biomedical applications including high biocompatibility, tailored bio-functionality, low immunogenicity, and *in vivo* stability for long-term usage remains very difficult.[5]

Covalently cross-linked hydrogels have limited application as injectable biomaterials because the mechanic stress applied through injection changes the network irreversibly or needs chemical re-connection.[6,7] The use of thermoresponsive *in situ* gelling hydrogels[8] represents another attractive avenue to circumvent the limitation of covalent networks because of the transient and reversible crosslinking mechanism.[9] It has allowed cell transplantation in mice via direct injection followed by monitoring material retention and cell retention for up to 3 weeks.[8]

However, *in situ* gelation in the human body can have adverse effects on the surrounding tissue if the gelation time is not adjusted to allow proper mixing, but still avoid diffusion of hydrogel components into the tissue.[10,11] Same is true for the degradation, if it occurs too quickly then insufficient scaffolding will remain to support tissue ingrowth, whereas a rate that is too slow will prevent proper tissue development and can promote fibrosis.[12,13] Moreover, non-covalent interactions between biomolecules are often very sensitive to subtle changes in chemical structures. Therefore, it is very challenging to modify a self-assembling

system including various biochemical moieties to mimic extracellular matrix (ECM) function or tuning drug release properties.[14] To overcome the difficulties associated with either covalent or non-covalent matrices, covalently conjugated hydrogel beads and self-assembled polymer-nanoparticles have been developed, which could be applied in wound healing and drug release over a period of few days.[13,15]

Another very important aspect for developing injectable biomaterials is to monitor the biomaterial with methods compatible with clinical practice. Whereas histological and biochemical analyses can illustrate the interaction between biomaterials and host tissue, characterization with high-resolution *in vivo* imaging technique such as MRI (magnetic resonance imaging)[16,17] and optical imaging, e.g., IR fluorescence imaging,[18,19] can provide information regarding the biomaterial *in vivo* non-invasively. Reference for µ-CT and stuff.[21,22] Such analyses could be particularly interesting for long-term monitoring, in which the native tissue and artificial material interact with each other over a period of weeks to months. Here we report a self-healing injectable hydrogel system, which rheological and biochemical properties can be tuned and the degradation can be monitored *in vivo* over a period up to 9 months by MRI and optical imaging using an IR fluorophore.

2. Results and Discussion

We have developed a hydrogel system cross-linked by the non-covalent interaction between negatively charged oligosaccharides (e.g. dextran sulfate (DS) or heparin) and peptide sequences containing $(BA)_n$ motif, where B is a basic residue (lysine or arginine), A is alanine, and n is the number of repeats.[22,23] The system was designed to resemble some important components in ECM such as glycosaminoglycan and matrix proteins motifs. While various highly sulfated oligosaccharides can be used, cell adhesive peptide can be conjugated to the $(BA)_n$ sequence without harming the gelation. The physical hydrogel showed high stability *in*

vitro (no detectable erosion after one year), and can be engineered using microfluidics to produce monodisperse beads as cell encapsulating micro-carriers,[23] Moreover, while the polymer network possesses large pore size allowing fast diffusion/release of proteins, a repertoire of conjugable tags based on the $(BA)_n$ motif has been developed, which can control the release of the resulting drug conjugates.[24] Importantly, the hydrogel is injectable, and extruding the hydrogel through a needle does not affect drug release.[24] Additionally, the hydrogels showed no cytotoxicity to embedded human neonatal dermal fibroblasts.[22,23] Given that neither the oligosaccharides nor the PEG-conjugated short synthetic peptides are expected to be strongly inflammatory,[25–27] we decided to test the injectable hydrogels in immunocompetent mice, and to monitor their erosion, inflammatory response and tissue remodeling, as well as the release of $(BA)_n$-tagged compounds.

2.1. Hydrogel design and *in vivo* hydrogel degradation

Hydrogels produced by mixing different peptide-starPEG conjugates and oligosaccharides differ widely on aspects of rheological properties and gelation rate.[22,23] We tested different combinations of $(BA)_n$-starPEG conjugates and negatively charged oligosaccharides and found that mixing KA5-starPEG with dextran sulfate (Gel-basic) led to optimal injectability. This means the hydrogels can be extruded from the syringe as stably gelated material (**Figure 1a**), but still show elasticity in a range of tissues, from soft tissue (as brain) to muscle.[28] A very important advantage of this system is that the resulting hydrogel can be injected shortly (30 min) after mixing the two precursors, while the hydrogel remains injectable even after 24 h. This feature allowed us to further fine-tune the injection condition in animal experiments, as shown in later part of this report.

As shown in figure **1a**, **Gel-basic** could be readily extruded through a needle. To investigate the effect of cell adhesive peptide on hydrogel-tissue interaction, the RGDSP peptide or its

scrambled sequence (GDPSR) was conjugated to the KA5 peptide, resulting in hydrogels **Gel-RGDSP** and **Gel-GDPSR**, respectively. To test drug release in whole animal live imaging experiment, the KA5-starPEG was premixed with IR fluorescent conjugate KA7-Cy7 before forming hydrogel with dextran sulfate (**Gel-Cy7**).

To investigate the hydrogel tissue interaction in vivo rather high concentration of starPEG and dextran sulfate (4 mM) and a high injection volume (100 µl) have been used to achieve optimal visualization of any inflammatory response and the hydrogel degradation. After injecting **Gel-basic**, **Gel-Cy7**, **Gel-RGDSP** and **Gel-GDPSR** into mice (100 µL each (Figure **1b**)), dedicated small animal MRI (7 T) was applied to visualize the hydrogels. Due to the larger amount of free water molecules in hydrogels (**Figure 2a**),[29,30] high signal intensity of the injected hydrogels allows distinguishing them from the surrounding native tissue. When the hydrogels were injected into mice 1.5 h after mixing the precursors, volume quantification has revealed a gradual increase of volume corresponding to high water content, reaching maximum after one day. For all the hydrogels tested previously[22–24] and investigated in this study, no swelling has been observed after gelation. The reason for the non-swelling behaviour is unknown and part of future studies. The increase of volume is therefore caused by the accumulation of interstitial fluid around the hydrogel. The influx of interstitial fluid was observed at all injection sites with **Gel-Cy7**, **Gel-RGDSP** and **Gel-GDPSR**, but not with **Gel-basic**. Three days post injection (p.i.), the volume reduced to the level of injected hydrogel. Interestingly, when the hydrogels were injected 18 h after mixing the precursors, the increase of volume was not detected (Figure **2a,b**). Additionally, after increasing the polymerization time to 18 h slower degradation could be observed for Gel-Cy7 and Gel-GDPSR (Figure **2c**).

The 1.5 h polymerized hydrogels were monitored *in vivo* by MRI for 9 months (Figure **2b**). The volumes of injected hydrogels reduced gradually over the long period of time, indicating their slow degradation *in vivo*. As expected, **Gel-basic** is more stable than **Gel-RGDSP** and

Gel-GDPSR. The KA5 peptide binds to the negatively charged oligosaccharide and the interaction prevents their digestion by proteases. The cell adhesive peptide RDGSP and its scrambled sequence GDPSR are not involved in direct interaction with dextran sulfate, thus more accessible to proteolysis.

To investigate whether the degradation of injected hydrogel is associated with enhanced local proteolysis activity, a matrix metalloproteinase (MMP)-sensitive fluorescent agent was used to visualize the MMP-activity around the hydrogels *in vivo* (Figure **2d**). The injected hydrogels did not cause remarkable increase of local MMP-mediated proteolysis, as compared with inflamed areas.[31] These results are in accordance with the findings of Ulbricht et al., 2014, who found out that PEG could be degraded hydrolytically under biological conditions. The degradation is obtained as oxidative degradation.[32] Therefore, the generation of reactive oxygen species could be involved in long-term biodegradability of PEG *in vivo*.[32]

2.2. *In vitro* characterization

To investigate the possible mechanism for the different *in vivo* degradation rates *in vitro* measurements of all hydrogels were carried out. We performed time-dependent rheological measurement after mixing peptide-starPEG and dextran sulfate, in the presence or absence of KA7-Cy7 (Figure **2e/f**). Interestingly, as compared to **Gel-basic**, while the time-dependent increase of storage modulus occurred with similar rates, the gel stiffness was remarkably increased by the presence of KA7-Cy7, whereas **Gel-RGDSP** and **Gel-GDPSR** are much softer. Given that self-healing is important for injectable materials for being able to recover the physicomechanical properties after removing the stress, we applied strong strain to break the hydrogel and measured the recovery of the storage modulus. As shown in figure **2e** and **2f**, in contrast to the slow gelation of freshly mixed precursors, instant recovery of hydrogel characteristic (G' >> G'') was observed for all four hydrogels of different compositions after

the applied strain was removed. The full recovery of stiffness occurred after about 20 min. The hydrogels become more opaque and porous which allows even better infiltration of cells into hydrogels (**Figure S4**).[13]

2.3. Release of tagged compound *in vivo*

Encapsulating IR fluorescent KA7-Cy7 in **Gel-basic** (**Gel-Cy7**) and visualization with optical imaging technique provided an alternative method to monitor the injected hydrogels *in vivo* non-invasively (**Figure 3a**). Moreover, the release of fluorescent conjugate can be followed, in addition to the information regarding volume quantification obtained via MRI.

To study the release of KA7 tagged compound *in vitro* (Figure **3b**), the KA7-fluorescein (KA7-Fluo) was used, because of the high sensitivity of measuring fluorescein using fluorescence spectrometer. Hydrogels were prepared by mixing KA5-starPEG, dextran sulfate, and KA7-Fluo. Interestingly, when 300 µL PBS was added to 10 µL KA7-Fluo loaded hydrogel of different gelation times (1.5 h or 18 h after mixing the precursors), remarkably different release profiles have been observed. Adding buffer to KA7-Fluo-loaded hydrogel caused a non-equilibrium condition and the compound was released during the first hours. Given that the supernatant was not changed throughout the experiment, the system reached the equilibrium gradually, as the rate of release became equal to the re-absorption of the dextran sulfate binding peptide.[24]

Moreover, a decrease of KA7-Fluo in solution after the initial release was observed for the 1.5 h gelated sample, indicating its reabsorption by hydrogel. Although the shortly gelated sample possesses all characteristic features of hydrogel, the non-covalently assembled network has not reached the thermodynamic equilibrium after 1.5 h. This also explains the difference between 1.5 and 18 h gelated samples in mice. The fast diffusion and release of components of a less stable hydrogel network could cause the accumulation of interstitial

8

fluid p.i. as well as relatively fast degradation, as compared with the hydrogel of 18 h gelation time.

In **Gel-Cy7** injected mice, after the initial release during the first 7 days, a slow and gradual decrease of fluorescence signal at the injection site was monitored for 9 months (Figure **3c**). To investigate whether the release correlates with the hydrogel degradation, the ratio of fluorescence intensity per volume was calculated (Figure **3c**). After the initial phase governed by Fickian diffusion, the KA7-Cy7 release and hydrogel degradation exhibited a good correlation until day 63. Starting from day 84 p.i., the decrease of fluorescence intensity exceeded the decrease of volume. As shown later in the histological analyses (**Figure 5**), the hydrogel degradation in later phase from day 14 onwards is also associated with the infiltration and growth of cells in the matrices.

2.4. Systemic hydrogel-tissue interaction

Injection of biomaterials may result in foreign body reactions that can lead to acute and chronic inflammatory responses and could cause adverse biomaterial-tissue interactions. We applied MRI to measure the size of inguinal lymph nodes in close proximity to the injected hydrogels (**Figure 4**).[33] Volume measurement of inguinal lymph nodes of untreated animals revealed lymph node sizes comparable to literature values of healthy immunocompetent mice.[34] Injection of TPA (12-O-Tetradecanoylphorbol-13-acetate), which induces a strong pro-inflammatory reaction, led to a significant increase in inguinal lymph node size as compared to the untreated animals, thus was used as positive control (Figure **4a/c**). The increase in lymph node size due to inflammatory response can also be found in literature.[35] Injecting hydrogels of different compositions did not cause significant increase in inguinal lymph node size compared to untreated animals (Figure **4b**/**c**).

To investigate the systemic hydrogel-tissue reaction further, the serum levels of the pro-inflammatory cytokines interleukin-6 (IL-6) and tumor necrosis factor-α (TNF-α) were measured. Serums of untreated and TPA injected animals were used as negative and positive controls, respectively. One day p.i. serum IL-6 levels in mice injected with hydrogels of different compositions had slightly increased as compared to the untreated control animals (Figure **4d**). However, the IL-6 levels in hydrogel injected animals did not significantly differ from the untreated negative control animals. The serum IL-6 concentrations in hydrogel treated mice decreased quickly to the level of untreated animals and were significantly less then in the TPA control animals from day 3 onwards. TNF-α is another essential component involved in most acute inflammatory responses. No significant difference in TNF-α serum levels among the mice treated with hydrogels of various compositions and untreated animals has been observed (Figure **4e**).

2.5. Cell migration into hydrogel and vascularization

To investigate local biomaterial-tissue interaction in more detail immunohistological staining of several marker proteins were performed (Figure **5**). CD68 is a pan-macrophages marker, while CD206 is specific for M2-macrophages. CD31 was used to illustrate the blood vessel formation. S100A4 is a marker of fibroblasts, complimentary to the van Gieson staining for collagen to illustrate the capsule formation around the injected hydrogels.

At 7 days p.i., CD68 and CD206 staining indicated that macrophages started to enter into the **Gel-RGDSP**, **Gel-GDPSR**, and **Gel-Cy7** (Figure **5a/b, 6a/b**). Macrophages were observed in **Gel-basic** hydrogels after 14 days (**Figure 6a/b**). This result is in good agreement with the relatively slow degradation of **Gel-basic** as observed in the MRI experiments. CD31 staining showed the formation of novel blood vessels at the border between hydrogel and native tissue (Figure **5c**). Interestingly, similar to the observation of macrophages, blood vessels could be

observed already at 7 days in **Gel-RGDSP**, **Gel-GDPSR**, and **Gel-Cy7** hydrogels, whereas CD31 staining could be observed in **Gel-basic** foremost after 14 days (Figure **5c**, **S6a**). Van Gieson staining and S100A4-positive staining after 7 days showed a moderate increase in the thickness of fibroblast layer, while the capsule around **Gel-RGDSP** was thicker than those of **Gel-basic**, **Gel-GDPSR**, and **Gel-Cy7** (Figure **5d, 6d, S6b**). The presence of cell adhesive sequence in **Gel-RGDSP** could induce the growth of fibroblasts on its boundary with native tissue. Cell proliferation measured by the staining of Ki67 was increased similar to the fibroblast and the blood vessel staining (**Figure S7c**). This result suggests that the majority of proliferating cells represent S100A4-positive fibroblasts and cells forming CD31-positive blood vessels.

Immunohistological evaluation over the long study period indicated that macrophages continue to enter into the hydrogel. The number of pan-macrophages and M2-macrophages of the injected hydrogel and surrounding tissue decreased gradually, due to the volume loss caused by degradation (Figure **6a/b**). CD68- and CD206-positive stained areas compared to the areas of all cell nuclei of the **Gel-basic** and **Gel-Cy7** injected tissues are larger than those of **Gel-RGDSP**, **Gel-GDPSR**. While blood vessels continued to grow into the hydrogel, the CD31 straining remained similar to the negative control (**Figure S7a**). The increase in fibroblast layer thickness during the first 1-2 weeks diminished to that of negative control over time (**Figure S7b**). Furthermore, staining of COX-2, a key inflammatory marker, remained low in all injected mice as compared with the negative control, confirming that all four hydrogels did not cause adverse inflammatory response (Figure **6c**). In summary, the gradual tissue remodeling around the injected hydrogels is associated with the slow loss of mass upon degradation (**Figure S8a**), cell infiltration (**Figure S8b**) as well as moderate activity of macrophages and angiogenesis. This is in good agreement with the absence of high local proteolysis and acute inflammatory responses illustrated by the *in vivo* imaging experiments.

3. Conclusion

Most polymer biomaterials cannot be injected into animals after gelation, thus must be transplanted through surgery.[36–38] To overcome such cumbersome procedure involving invasive operation, novel injectable biomaterials such as hydrogel beads have been developed as precursors, which could be interconnected to achieve enhanced self-healing properties for injection experiments.[13] In this work, we present a fundamentally different approach by using non-covalently assembled matrix as injectable hydrogels. The straightforward mix and inject nature of this method can be easily applied in a broad range of preclinical models and experimental settings without the need for *in situ* gelation. Moreover, by applying small animal MRI, the hydrogels have been visualized and monitored *in vivo* without any labeling or the use of contrast agents over a long experimental period (up to 9 months). This approach is in accordance to the principles reduction and refinement in animal research. In combination with *ex vivo* and immunohistological analysis, we have demonstrated that the injected matrices underwent slow degradation and were replaced gradually by native tissue. By the use optical imaging *in vivo* using an IR fluorophore, an affinity captured compound has shown a controlled release from hydrogel over a time period of 9 months. The facile synthesis, high biocompatibility and stability of this injectable non-covalent matrix system could lead to various experimental and clinical applications in regenerative medicine and drug delivery.

4. Experimental Section

Peptide synthesis

For peptide synthesis all required chemicals were purchased from IRIS Biotech GmbH (Marktredwitz, Germany) unless otherwise specified (see supplementary information). All

peptides (see Table **S1**) were prepared using standard fluorenylmethyloxycarbonyl (Fmoc) chemistry on a solid-phase with 2-(1H-benzotriazol-1-yl)-1,1,3,3-tetramethyluronium hexafluorphosphate (HBTU) activation on an automated solid-phase peptide synthesizer (ResPep SL, Intavis, Cologne, Germany). To ensure good peptide quality each amino acid was coupled twice with each five times excess and all non-reacted amino groups were capped with acetic anhydride. Peptide purification was performed via reverse-phase HPLC on a preparative HPLC (ProStar, Agilent Technologies, Santa Clara, USA) equipped with a preparative reverse-phase C18 column (AXIA 100A, Phenomenex, Torrance, CA, USA). Purity was confirmed (see **Figure S1**) by analytical reverse phase UPLC using an analytical reverse phase C18 column, applying an isocratic gradient and electrospray ionization mass spectrometry (ACQUITY system, Waters, Milford MA, USA). The peptide was lyophilized to a white fluffy powder and stored at 4°C under dry conditions for not more than 1 week before further coupling.

Labeling of peptide

The coupling of fluorophores to the peptides was performed using Michael-type addition reactions between maleimide-functionalized fluorescein (Sigma-Aldrich Co. LLC., St. Louis, MO, USA) and Cy7 (Lumiprobe, Hannover, Germany) and cysteine-terminated KA7 peptide. KA7 was dissolved in PBS (pH 7.4), the fluorophore in DMSO and they were mixed in a molar ratio of 1:2 (fluorophore:peptide) with a total concentration of 80 mg/mL. The reaction mixture was quickly sealed and stirred on a stirring plate at 750 rpm at room temperature (24°C) for 2 h. The crude product was purified as described in chapter peptide synthesis.

Synthesis of peptide-starPEG conjugates

The synthesis of the peptide-starPEG conjugates utilized in hydrogel assembly was conducted via Michael-type addition reactions between 10 kDa maleimide functionalized four-arm

polyethylene glycol (starPEG, JenKem Technology, Beijing, China) and cysteine-terminated peptides from the library. Both components were dissolved in PBS (pH 7.4) and mixed in a molar ratio of 1:5 (starPEG:peptide) with a total concentration of 80 mg/mL. The reaction mixture was quickly sealed and stirred on a stirring plate at 750 rpm at room temperature (24°C) for 2 h. The crude product was dialyzed to remove uncoupled peptides and salt in a dialysis tube with an 8 kDa cut off (Spectrum Laboratories, Inc., Rancho Dominguez, CA, USA) against 10 l water under constant water exchange for 2 days. Afterwards the product was analyzed by reverse phase UPLC (ACQUITY system, Waters, Milford MA, USA) using an analytical reverse phase C18 column column for protein separation (Phenomenex, Torrance, CA, USA) and an isocratic gradient (see **Figure S2**). The dialyzed product in water was lyophilized.

Assembly of hydrogel networks

Peptide-starPEG conjugate, 5 kDa dextran sulfate (Sigma-Aldrich Co. LLC., St. Louis, MO, USA), KA7-Cy7 and KA7-Fluo were solved in PBS (pH 7.4) and filtered through a 0.22 μm centrifuge tube filter. These solutions were mixed (by vortexing) in a volume ratio of 7:1:2 (KA5-starPEG conjuate:KA7-Cy7 or KA7-Fluo:dextran sulfate) to yield 4 mM KA5-starPEG conjuate, 4 mM dextran sulfate and 0.4 mM KA7-Cy7 or KA7-Fluo. Additionally, solutions were mixed (by vortexing) in a volume ratio of 8:2 (peptide-starPEG conjuate:dextran sulfate) to yield 4 mM peptide-starPEG conjuate. These hydrogel mixtures were further used.

Nomenclature of hydrogels:

Gel-basic: 4 mM KA5-starPEG, 4 mM 5 kDa dextran sulfate

Gel-Cy7:   4 mM KA5-starPEG, 4 mM 5 kDa dextran sulfate, 0.4 mM KA7-Cy7

Gel-RGDSP: 4 mM KA5-RGDSP-starPEG, 4 mM 5 kDa dextran sulfate

Gel-GDPSR: 4 mM KA5-GDPSR-starPEG, 4 mM 5 kDa dextran sulfate

The water percentage in these hydrogels is the following:

14

Gel-basic: 91.7% (8.3% solid content)

Gel-Cy7: 91.6% (8.4% solid content)

Gel-RGDSP: 90.7% (9.3% solid content)

Gel-GDPSR: 90.7% (9.3% solid content)

Gelation time analysis

Gelation time of hydrogels was characterized using a stress-controlled rheometer at 20°C and a conical geometry with 49.955 mm in diameter, an angle of 0.996° and truncation of 52 μm (Physica MCR 301, Anton-Paar, Ashland, VA, USA). All hydrogels were incubated using an almost closed environment around the geometry to avoid evaporation. The stiffness was measured every 5 minutes using 1 Hz frequency and 2% amplitude. All experiments were repeated 2 times and the average was plotted.

Analysis of peptide release from hydrogel

Hydrogel with KA7-Fluo was prepared (see section assembly of hydrogel networks) and 15 times 10 μL pipetted in a 96 well plate before gelation. After 1.5 or 18 h 300 μL PBS was added. The well plates were airtight closed using an adhesive black light absorbing film and incubated at 37°C. The peptide release was analysed through the not hydrogel covered transparent bottom of the plate measuring the fluorescence intensity using a plate reader (PARADIGM Detection platform, Beckman Coulter, Brea, CA, USA). The experiment was prepared twice at two different days.

Hydrogel injection

Animal experiments were performed in accordance with the guidelines of the German Regulations for Animal Welfare. The protocol was approved by the local Ethical Committee for Animal Experiments. Gelation of all hydrogels was started 1.5 h before injection, if not

referred otherwise. Therefore, female immunocompetent SKH1-Elite mice were purchased from Charles River. SKH1 mice (age 6-8 weeks, weight 22-30 g) were injected with either 100 µL **Gel-basic** on the left site and 100 µL of **Gel-Cy7** on the right site or with 100 µL **Gel-RGDSP** on the left site and 100 µL of **Gel-GDPSR** on the right site of the lower back of each animal. For the injection a 1 mL Luer-Lock syringe and 3 cm long needle with 0.6 mm inner diameter was used (B. BRAUN Melsungen AG, Melsungen, Germany).

Volume determination measurements in vivo

The volume of the injected hydrogels and the inguinal lymph nodes was determined using 7 T small animal magnetic resonance imaging (MRI, Bruker) with a T2 weighted measuring sequence. The relaxation time was 38 ms. Using a field of view of 4×4 cm and a matrix of 256×256 px the final resolution was 156 µm in xy-direction and, as determined by the slice thickness 800 µm in z-direction. For quantification of the hydrogel volume the software ROVER (ABX GmbH) was used.

In vivo fluorescence imaging

For quantification of remaining Cy7 at the site of injection of the **Gel-Cy7** hydrogel *in vivo* fluorescence imaging was performed. Therefore, the small animal optical imaging device *in vivo Xtreme* (Bruker) was used. For detection of Cy7 the filter set with an excitation filter of 750 nm and an emission filter of 790 nm wavelength was chosen. MMP activity was determined using MMP-Sense 680 (Perkin Elmer, 650/700 nm). 24 h after intravenous (i.v.) injection of 100 µL MMP-Sense 680, fluorescence was assessed using optical imaging. Exposure time for fluorescence images was 4 s. As reference for quantification, a channel with no specific fluorescence GFP (480/535 nm) was chosen and an image with an exposure time of 4 s was acquired. As anatomical reference channel X-ray was performed with an acquisition time of 1.2 s and energy of 45 keV.

For the acquisition and quantification of images Bruker Molecular Imaging software version 7.2 was used. For fluorescence images, net fluorescence intensity was determined. To minimize quantification of unspecific auto-fluorescence, fluorescence images were divided by the reference channel before quantifying the intensity. To further investigate if the release of the hydrogel is in accordance with the degradation of hydrogel the ratio of net fluorescence intensity to the volume was calculated.

Serum sample preparation and analysis

To every time point of histological sample preparation serum samples of the twice injected (**Gel-basic** and **Gel-Cy7** or **Gel-RGDSP** and **Gel-GDPSR**) were collected. As negative control untreated SKH1 mice were used. As inflammation positive control mice were injected with 12-O-Tetradecanoylphorbol-13-acetate (TPA) as published elsewhere.[39] The injection of TPA leads to the activation of NF-κB and therefore to pro-inflammatory reactions.[40,41] At selected time points and once for both control mice groups whole blood samples were collected by heart puncture of 3 anesthetized mice for each group and allowed to clot for 30 min at room temperature. Samples were centrifuged at $2,000 \times g$ for 15 min at 4°C. The supernatant was transferred into a fresh tube and snap frozen in liquid nitrogen immediately. Serum was stored at −65°C until further investigation. IL-6 and TNFα levels of serum samples were quantified using IL-6 mouse ELISA-Kit (R&D Systems, M600B) and a TNFα mouse ELISA-Kit (Abcam, ab100747).

Histological analysis

Preparation of cryo-sections was performed as published before.[39] For histological analysis 3 animals per group were sacrificed at the selected time points. The hydrogels were surgically removed including the surrounding tissue. The tissues were fixed in 4% (w/v) PFA for 24 h at room temperature and incubated for 3 days in 20% (w/v) sucrose solution in phosphate

buffered saline (PBS) at 4°C. Tissue samples were snap frozen and stored at −65°C. For cryosectioning samples were cut right through the middle of the remaining hydrogel piece. Samples were embedded in 7.5% (w/v) gelatin solution with 20% (w/v) sucrose in PBS, frozen, and cut at 10 µm thickness using a cryostat at −30°C. Histological samples were stained by hematoxylin & eosin (H&E) using standard protocols. Specific tissue response was visualized using immunohistological staining for different cell markers, which are summarized in **Table 1**.

Biotinylated secondary antibodies were used. After incubation with ExtrAvidin peroxidase (Sigma-Aldrich), staining was visualized using AEC substrate kit (BD Biosciences). Sections were counterstained using Mayer's hematoxylin. Images were acquired using AxioImager.A1 and the appropriate software package AxioVision (Carl Zeiss).

Quantification of immunohistological stainings was performed for sections of three different animals per time point using FIJI.[42] Therefore the color threshold plugin was used. RGB values were set for cell nuclei and for immunohistological positive stained areas. After applying the analyze particles plugin positive stained area was divided by area of cell nuclei.

To measure capsule thickness of the implanted hydrogels Van Gieson's staining was performed using standard protocols. Therefore, cell nuclei were stained using Weigert's iron hematoxylin solution. Collagen was stained using Van-Gieson-mixture consisting of saturated picric acid and 1% (w/v) thiazine red. For the measurement of capsule thickness AxioVision (Carl Zeiss) software was used. Capsule thickness was measured for sections of three different animals per time point. For each section 5 points on each capsule-site (the skin- and muscle-site) around the implant were measured (**Figure S9**).

Statistical analysis

Statistical significance of hydrogel and inguinal lymph node volume as well as for the ELISA analysis, FACS analysis, and histological investigations over the time course was calculated

using a two-way ANOVA followed by a Bonferroni post hoc test using Prism 6 (GraphPad Software). Statistical significance was assumed for $p < 0.05$, $p < 0.001$ for all statistical analysis.

Supporting Information

Supporting Information is available from the Wiley Online Library or from the author.

Acknowledgements

Contributions

C.T. and R.W. contributed equally to this study. J.P. and Y.U. share senior authorship. The study presented here was carried out in collaboration between all authors. R.W. and Y.Z. provided the hydrogels. R.W., Y.Z. and C.W. contributed their physicochemical analyses. C.T., R.W., Y.Z. and J.P. conceived and designed the experiments, carried out the experiments, analyzed/interpreted the data, and wrote the manuscript. C.T. carried out the hydrogel injections, the MRI and optical imaging experiments *in vivo*. E.R. carried out the immunohistological evaluation of tissue sections, which was part of her master thesis at the Technische Universität Dresden, Department of Biology. All authors have read and approved the final manuscript.

Competing interests

R.W. and Y.Z. are inventors on a patent application covering the described hydrogel technology.

References

[1] M. J. Webber, E. A. Appel, E. W. Meijer, R. Langer, *Nat. Mater.* **2015**, *15*, 13.

[2] Y. Lin, D. Jiandong, *Chem. Soc. Rev.* **2008**, *37, 1473.*

[3] W. E. Hennink, C. F. van Nostrum, *Adv. Drug Deliv. Rev.* **2012**, *64*, 223.

[4] C. Tianyuan, C. Liang, Y. Lin, D. Jiandong, *Sci. Rep.* **2014**, *4, 5473.*

[5] D. Seliktar, *Science* **2012**, *336*, 1124.

[6] M. Patenaude, N. M. B. Smeets, T. Hoare, *Macromol. Rapid Commun.* **2014**, *35*, 598.

[7] F. Ding, S. Wu, S. Wang, Y. Xiong, Y. Li, B. Li, H. Deng, Y. Du, L. Xiao, X. Shi, *Soft Matter* **2015**, *11*, 3971.

[8] L. Cai, R. E. Dewi, A. B. Goldstone, J. E. Cohen, A. N. Steele, Y. J. Woo, S. C. Heilshorn, *Adv. Healthc. Mater.* **2016**.

[9] H. Wang, S. C. Heilshorn, *Adv. Mater.* **2015**, *27*, 3717.

[10] J. A. Yang, J. Yeom, B. W. Hwang, A. S. Hoffman, S. K. Hahn, *Prog. Polym. Sci.* **2014**, *39*, 1973.

[11] M. N. Collins, C. Birkinshaw, *Carbohydr. Polym.* **2013**, *92*, 1262.

[12] J. Alijotas-Reig, M. T. Fernández-Figueras, L. Puig, *Clin. Rev. Allergy Immunol.* **2013**, *45*, 97.

[13] D. R. Griffin, W. M. Weaver, P. O. Scumpia, D. Di Carlo, T. Segura, *Nat. Mater.* **2015**, *14*, 737.

[14] M. Guvendiren, H. D. Lu, J. A. Burdick, *Soft Matter* **2012**, *8*, 260.

[15]   E. A. Appel, M. W. Tibbitt, M. J. Webber, B. A. Mattix, O. Veiseh, R. Langer, *Nat. Commun.* **2015**, *6*, 1.

[16]   S. M. Dorsey, J. R. McGarvey, H. Wang, A. Nikou, L. Arama, K. J. Koomalsingh, N. Kondo, J. H. Gorman, J. J. Pilla, R. C. Gorman, J. F. Wenk, J. A. Burdick, *Biomaterials* **2015**, *69*, 65.

[17]   A. Berdichevski, H. Simaan Yameen, H. Dafni, M. Neeman, D. Seliktar, *Proc. Natl. Acad. Sci.* **2015**, *112*, 201502232.

[18]   N. Artzi, N. Oliva, C. Puron, S. Shitreet, S. Artzi, A. Bon Ramos, A. Groothuis, G. Sahagian, E. R. Edelman, *Nat. Mater.* **2011**, *10*, 704.

[19]   B. W. Xie, I. M. Mol, S. Keereweer, E. R. van Beek, I. Que, T. J. A. Snoeks, A. Chan, E. L. Kaijzel, C. W. G. M. Löwik, C. W. Lowik, *PLoS One* **2012**, *7*, e31875.

[20]   L. Kewen, M. Qian, Y. Lin, D. Jiandong, *J. Mater. Chem. B* **2016**, 4, 7793.

[21]   L. Kewen, S. Wenjia, C. Luping, Y. Lin, D. Jiandong, *Chem. Commun.* **2015**, 51, 6080.

[22]   R. Wieduwild, M. Tsurkan, K. Chwalek, P. Murawala, M. Nowak, U. Freudenberg, C. Neinhuis, C. Werner, Y. Zhang, *J. Am. Chem. Soc.* **2013**, *135*, 2919.

[23]   R. Wieduwild, S. Krishnan, K. Chwalek, A. Boden, M. Nowak, D. Drechsel, C. Werner, Y. Zhang, *Angew. Chem. Int. Ed. Engl.* **2015**, *54*, 3962.

[24]   R. Wieduwild, W. Lin, A. Boden, K. Kretschmer, Y. Zhang, *Biomacromolecules* **2014**, *15*, 2058.

[25]   C. R. Ricketts, K. W. Walton, *Br. J. Pharmacol.* **1953**, *8*, 476.

[26]   C. V. Rao, *An Introduction to Immunology*, Alpha Science International Ltd., Pangbourne, **2002**.

[27]   H. Schellekens, W. E. Hennink, V. Brinks, *Pharm. Res.* **2013**, *30*, 1729.

[28]   D. E. Discher, D. J. Mooney, P. W. Zandstra, *Science* **2009**, *324*, 1673.

[29]   N. A. Peppas, P. Bures, W. Leobandung, H. Ichikawa, *Eur. J. Pharm. Biopharm.* **2000**, *50*, 27.

[30] A. S. Hoffman, *Adv. Drug Deliv. Rev.* **2012**, *64*, 13.

[31] J. M. Ibarra, F. Jimenez, H. G. Martinez, K. Clark, S. S. Ahuja, *Int J Inflam* **2011**, *2011*, 691587.

[32] J. Ulbricht, R. Jordan, R. Luxenhofer, *Biomaterials* **2014**, *35*, 4848.

[33] Z. Zhang, D. Procissi, W. Li, D.-H. Kim, K. Li, G. Han, Y. Huan, A. C. Larson, *J. Immunol. Methods* **2013**, *400*, 23.

[34] V. Economopoulos, J. C. Noad, S. Krishnamoorthy, B. K. Rutt, P. J. Foster, *PLoS One* **2011**, *6*, e27508.

[35] S. T. Proulx, E. Kwok, Z. You, M. O. Papuga, C. A. Beck, D. J. Shealy, C. T. Ritchlin, H. A. Awad, B. F. Boyce, L. Xing, E. M. Schwarz, *Arthritis Rheum.* **2007**, *56*, 4024.

[36] B. D. Ratner, S. J. Bryant, *Annu. Rev. Biomed. Eng.* **2004**, *6*, 41.

[37] S. J. Hollister, *Adv. Mater.* **2009**, *21*, 3330.

[38] E. T. Pashuck, M. M. Stevens, *Sci. Transl. Med.* **2012**, *4*, 160sr4.

[39] S. Ullm, A. Krüger, C. Tondera, T. P. Gebauer, A. T. Neffe, A. Lendlein, F. Jung, J. Pietzsch, *Biomaterials* **2014**, *35*, 9755.

[40] J. K. Kundu, Y. K. Shin, Y. J. Surh, *Biochem. Pharmacol.* **2006**, *72*, 1506.

[41] J. K. Kundu, Y. K. Shin, S. H. Kim, Y. J. Surh, *Carcinogenesis* **2006**, *27*, 1465.

[42] J. Schindelin, I. Arganda-Carreras, E. Frise, V. Kaynig, M. Longair, T. Pietzsch, S. Preibisch, C. Rueden, S. Saalfeld, B. Schmid, J.-Y. Tinevez, D. J. White, V. Hartenstein, K. Eliceiri, P. Tomancak, A. Cardona, *Nat. Methods* **2012**, *9*, 676.

[43] M. Hayashi, A. Majumdar, X. Li, J. Adler, Z. Sun, S. Vertuani, C. Hellberg, S. Mellberg, S. Koch, A. Dimberg, G. Y. Koh, E. Dejana, H.-G. Belting, M. Affolter, G. Thurston, L. Holmgren, D. Vestweber, L. Claesson-Welsh, *Nat. Commun.* **2013**, *4*, 1.

[44] F. O. Martinez, S. Gordon, *F1000Prime Rep.* **2014**, *6*.

[45] T. Scholzen, J. Gerdes, *J. Cell. Physiol.* **2000**, *182*, 311.

[46] J. Zhang, L. Chen, X. Liu, T. Kammertoens, T. Blankenstein, Z. Qin, *Cancer Res.*

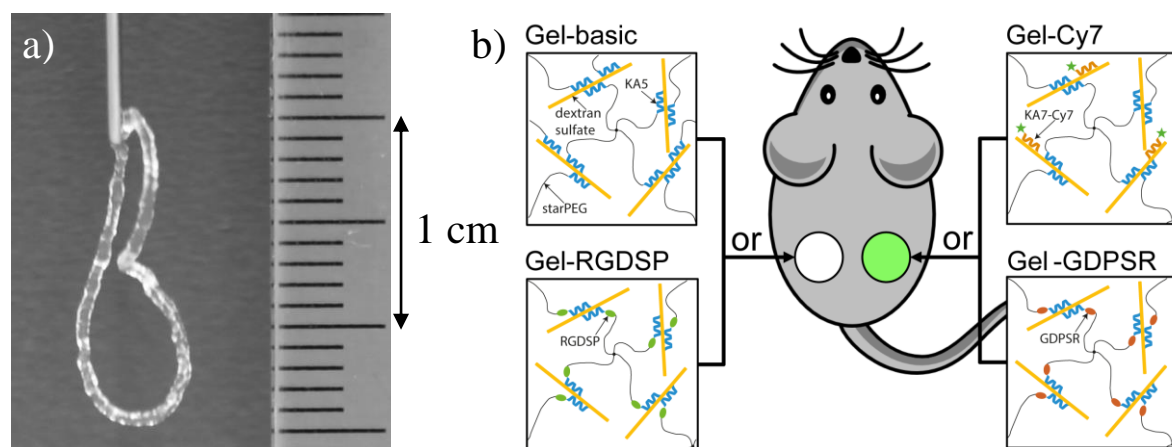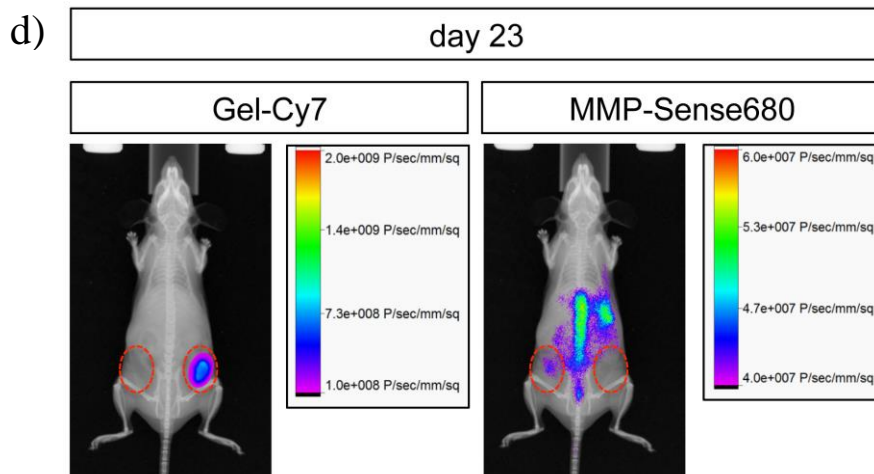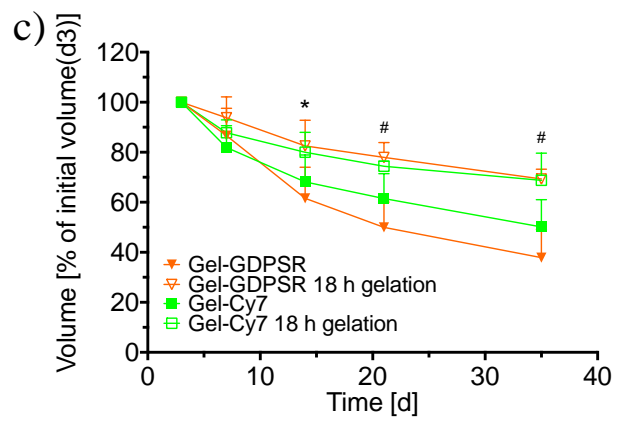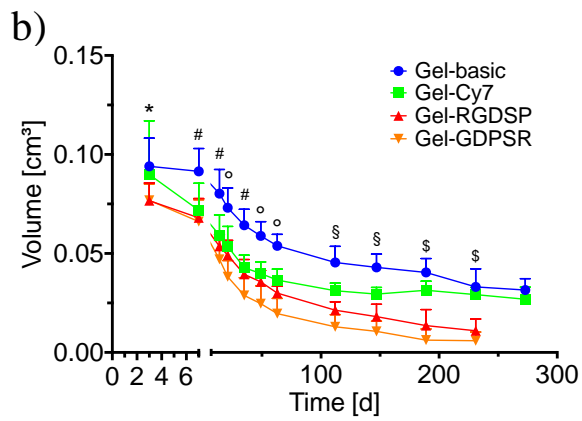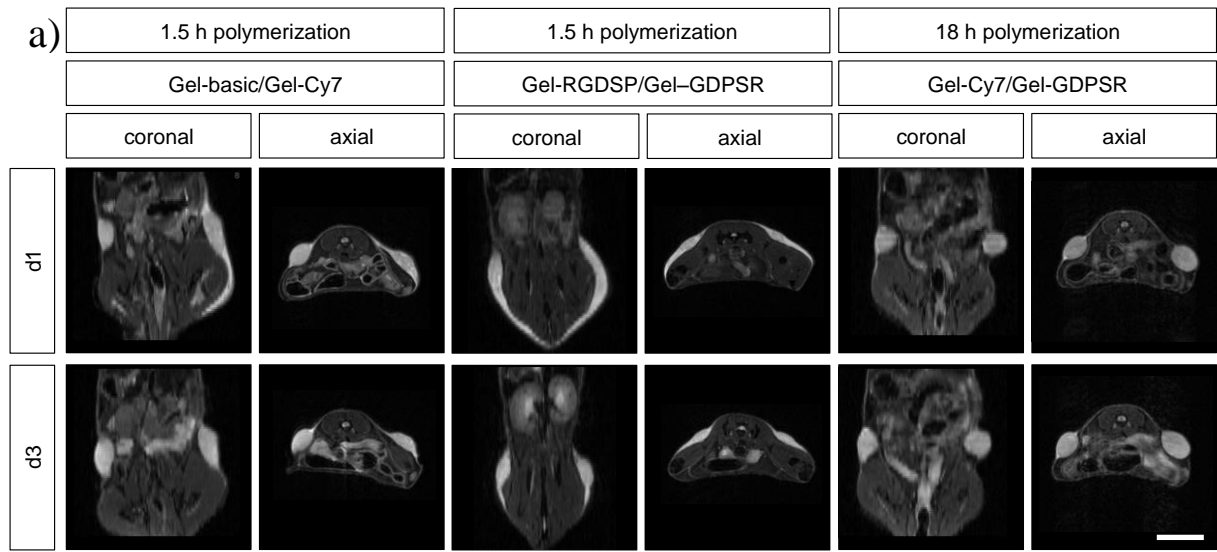**Figure 1.** Hydrogel integrity after extrusion and composition of injected hydrogel into SKH1-Elite mice. (**a**) **Gel-basic** prepared in a 250 µL syringe with gauge G22 needle and could be readily extruded 1.5 h after preparation. (**b**) Scheme of injection of mice. Animals were subcutaneously injected in the lower dorsal area with either 100 µL **Gel-basic** on the left site and **Gel-Cy7** on the right site or the same volume of **Gel-RGDSP** on the left site and **Gel-GDPSR** on the right site. All hydrogels were prepared in PBS (pH 7.4). Hydrogel compositions: **Gel-basic:** 4 mM KA5-starPEG, 4 mM 5 kDa dextran sulfate; **Gel-Cy7:** 4 mM KA5-starPEG, 4 mM 5 kDa dextran sulfate, 0.4 mM KA7-Cy7; **Gel-RGDSP:** 4 mM KA5-RGDSP-starPEG, 4 mM 5 kDa dextran sulfate; Gel-GDPSR: 4 mM KA5-GDPSR-starPEG, 4 mM 5 kDa dextran sulfate.
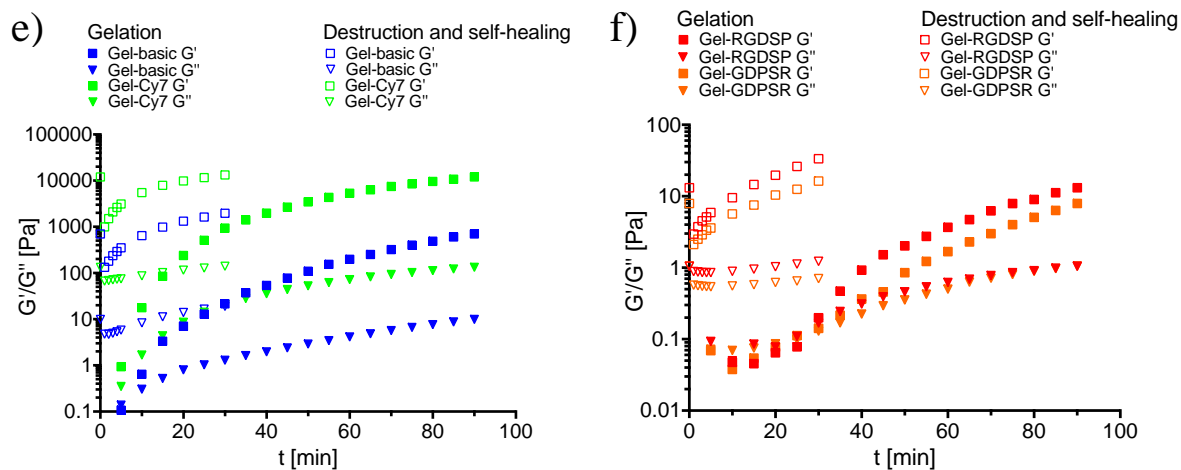
a)

1.5 h polymerization		1.5 h polymerization		18 h polymerization	
Gel-basic/Gel-Cy7		Gel-RGDSP/Gel–GDPSR		Gel-Cy7/Gel-GDPSR	
coronal	axial	coronal	axial	coronal	axial

b)

c)

d)

day 23

Gel-Cy7

MMP-Sense680

Figure 2. Hydrogel volume and degradation rate was determined using small animal MRI. (**a**) Visualization of hydrogel using dedicated small animal MRI with a T2 weighted TRARE measuring sequence. Compared are hydrogel volumes and body liquid accumulation after hydrogel injection of 1.5 h gelated **Gel-basic**, **Gel-Cy7**, **Gel-RDGSP** and **Gel-GDPSR** and 18 h gelated **Gel-Cy7** and **Gel-GDPSR** 1 and 3 days post injection (p.i.). Scale bar: 1 cm. (**b**) Graphical visualization of hydrogel volume determined by MRI over time of mice injected 1.5 h after hydrogel preparation (n=8-10, mean + s.d.). Values of day 0 and 1 were excluded, because body liquid accumulation (see (**a**)) at these days made it impossible to distinguish body liquid and hydrogel. Statistical significant differences with $p<0.05$ were determined using two-way ANOVA with Bonferroni *post hoc* test: * **Gel-basic** vs. **Gel-RGDSP/Gel-GDPSR**; # **Gel-basic** vs. all others; ° **Gel-basic** vs. all others and **Gel-Cy7** vs. **Gel-GDPSR**; § Gel-basic vs. **Gel-RGDSP/Gel-GDPSR** and **Gel-GDPSR** vs. **Gel-basic/Gel-Cy7**; $ Gel-basic/Gel-Cy7 vs. **Gel-RGDSP/Gel-GDPSR**. (**c**) same as (**b**) but comparing hydrogel injected into mice after 1.5 h and 18 h. * **Gel-GDPSR** vs. **Gel-GDPSR 18 h**; # **Gel-GDPSR** vs. **Gel-GDPSR 18 h** and **Gel-GDPSR** vs **Gel-Cy7 18 h**. Analysis of hydrogel gelation and self-healing properties *in vitro*. For hydrogel composition see **figure 1**. (**d**) MMP specific fluorescence agent MMP-Sense 680 (λ_{ex}=650 nm, λ_{em}=700 nm) showed no specific fluorescence 23 days after **Gel-basic** and **Gel-Cy7** injection. Gelation and self-healing properties of (**e**) **Gel-basic** and **Gel-Cy7** and (**f**) **Gel-RGDSP** and **Gel-GDPSR** are shown. A

rheometer with conical geometry was used. For the gelation time elastic modulus was measured every 5 min. For self-healing analysis hydrogel gelated for 1.5 h was destroyed and recovery measured every minute until 5 min and then every 5 min until 25 min after destruction. Hydrogel showed immediately after destruction solid properties and recovered to initial elastic modulus (equal to 1.5 h gelation) after 20 min.
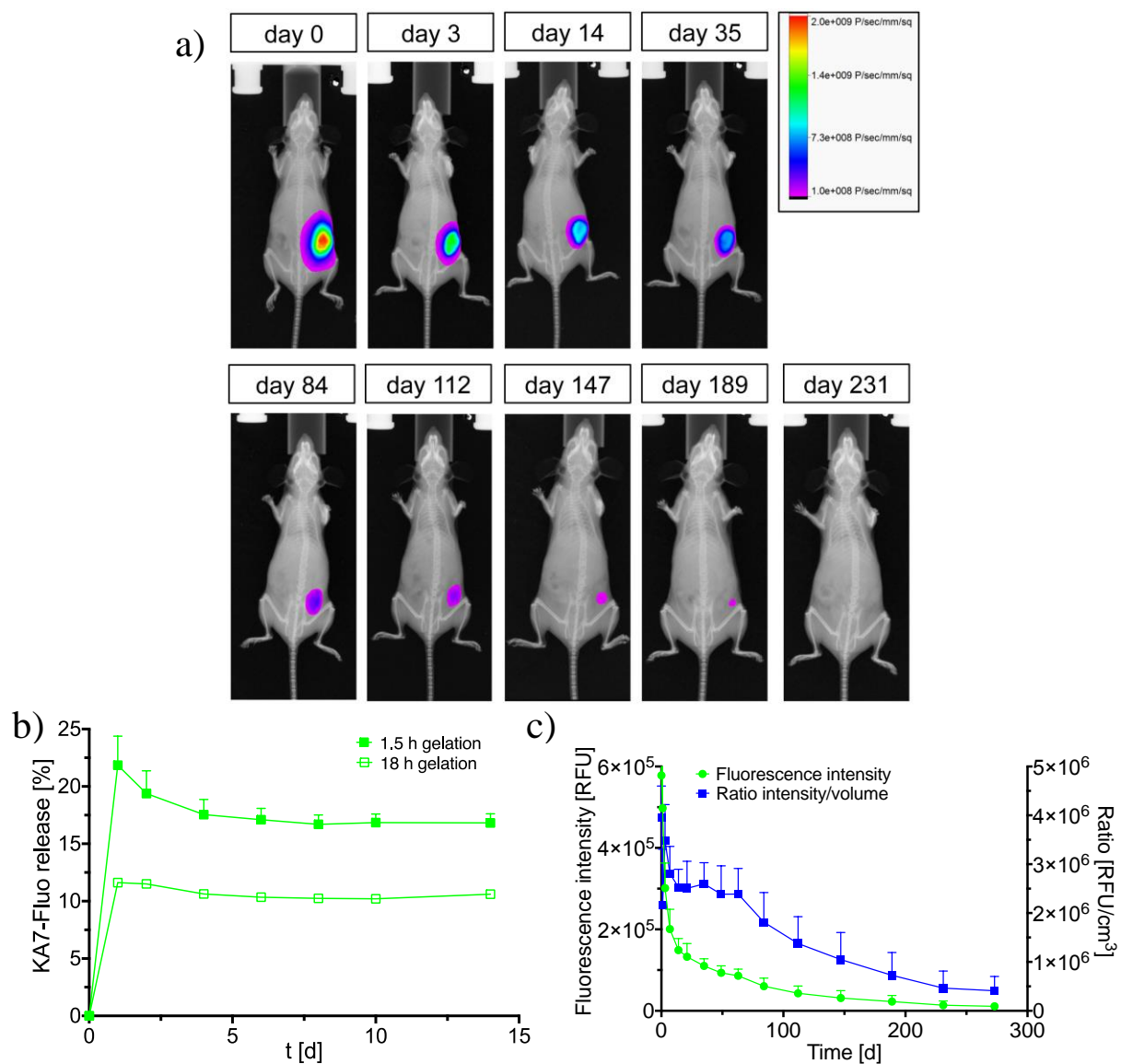
Figure 3. (**a**) Representative fluorescence images (λ_{ex}=750 nm, λ_{em}=790 nm) of **Gel-basic** and **Gel-Cy7** injected mice is shown. Specific fluorescence signal was observed at the injection site of **Gel-Cy7** but not **Gel-basic**. Signal intensity decreased with increasing time. (**b**) *In vitro* release analysis of KA7-Fluo loaded hydrogel (instead of KA7-Cy7 in **Gel-Cy7**). Change of fluorophore was needed because of better sensitivity of fluorescence spectrometer at this wavelength. 10 µL hydrogels were incubated for 1.5 h or 18 h before adding 300 µL supernatant and fluorescent intensity measured in supernatant without changing supernatant (mean + s.d.). (**c**) KA7-Cy7 release was quantified using optical imaging (green line; n=8,

mean + s.d.). Ratio of remaining fluorescence intensity to the hydrogel volume was calculated
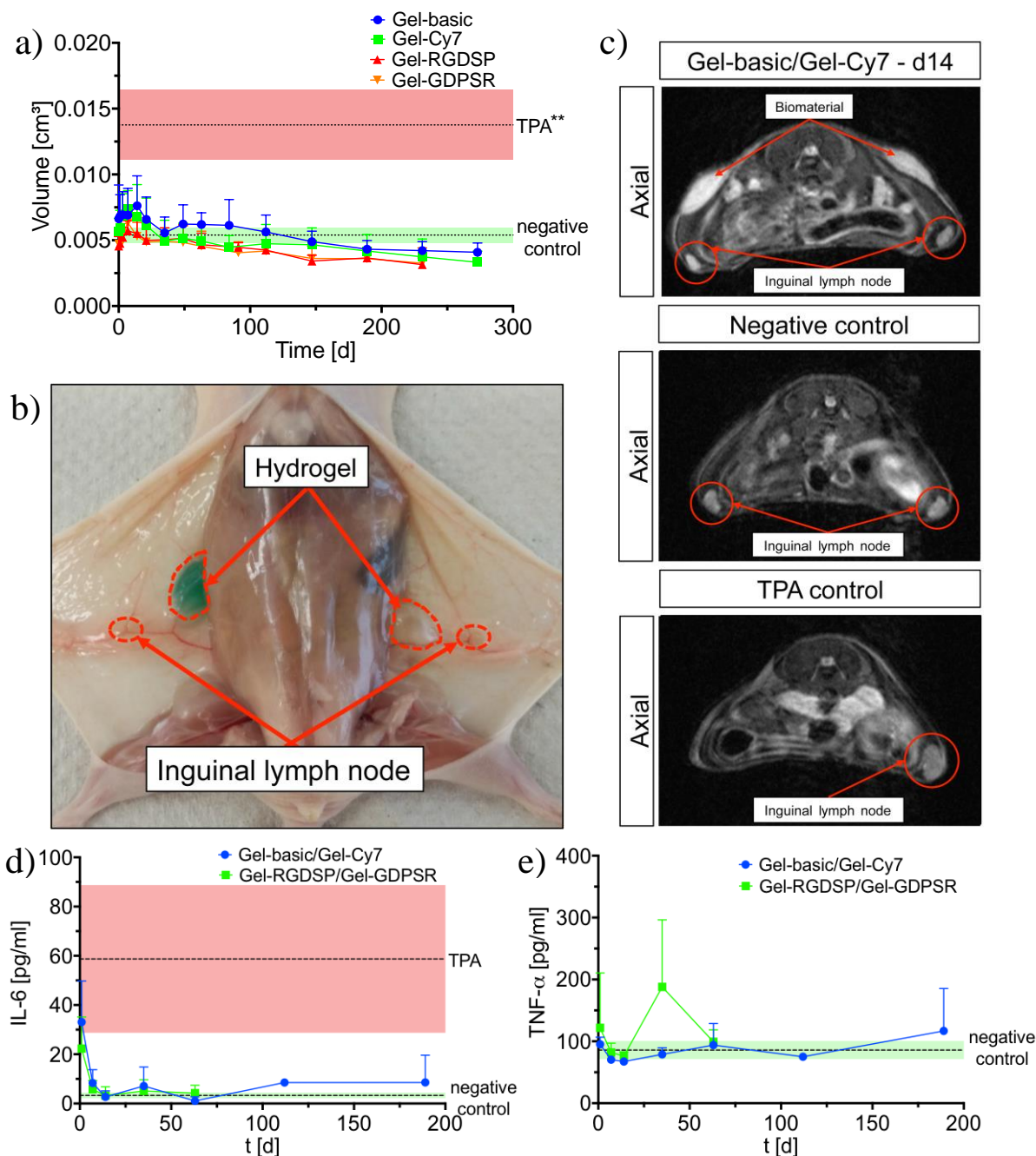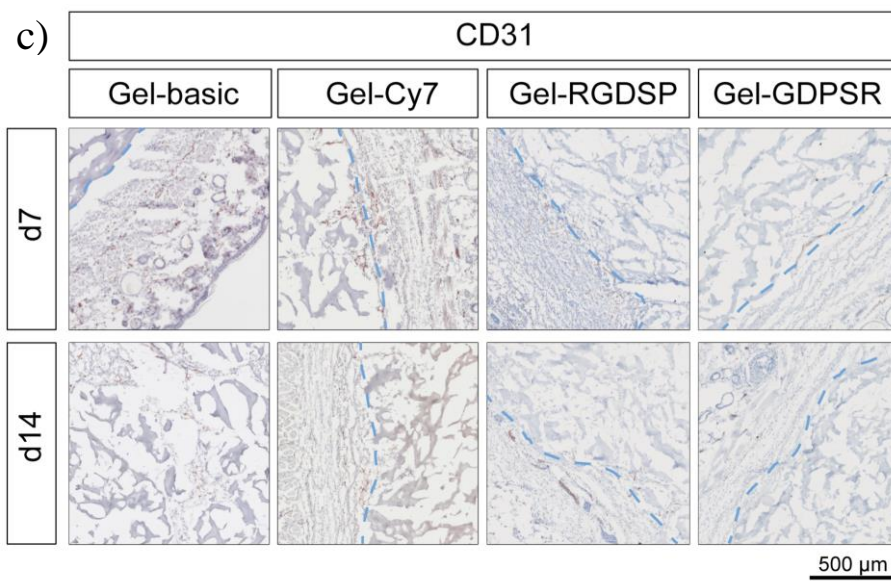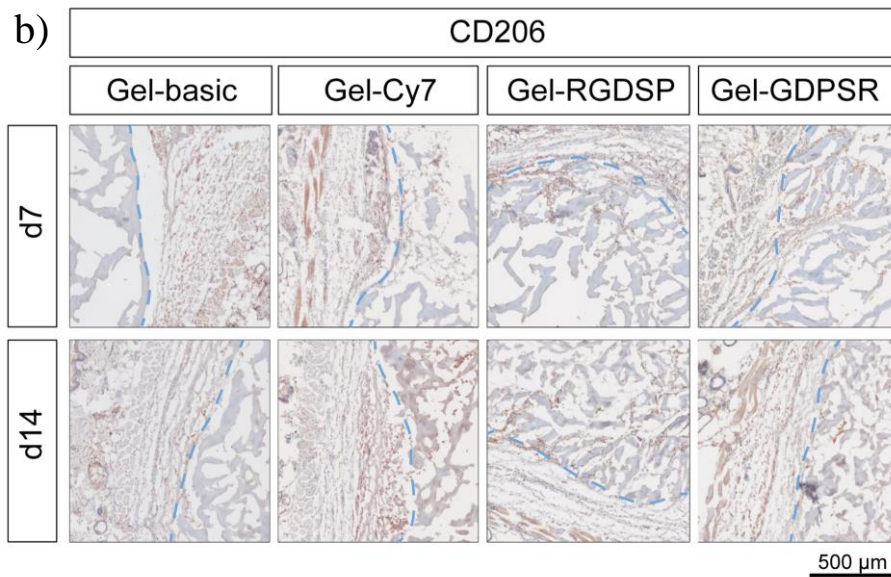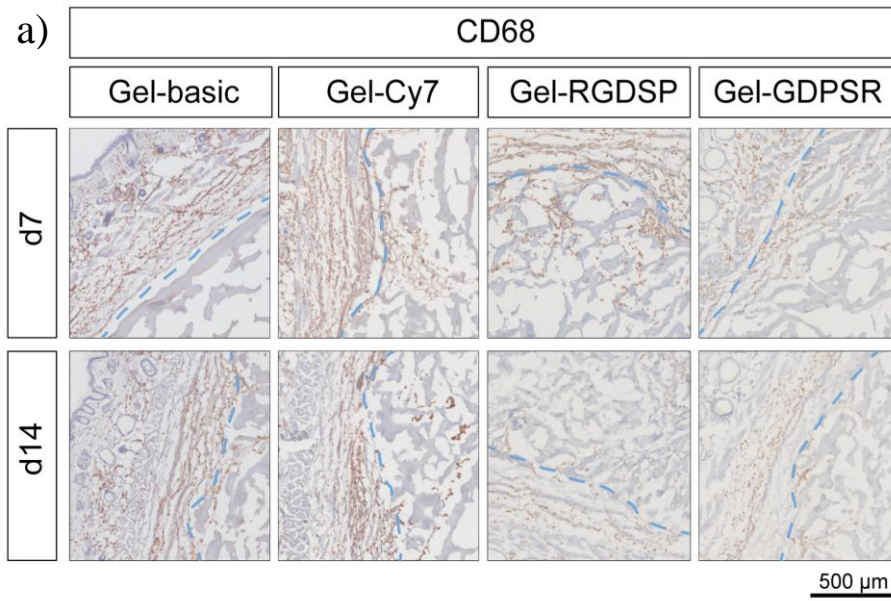
(blue line; n=8, mean + s.d.).

Figure 4. (**a**) Quantification of the volume of inguinal lymph nodes located next to **Gel-basic**, **Gel-Cy7**, **Gel-RGDSP**, and **Gel-GDPSR** is shown. Untreated (green area, n=6, mean ± s.d.) and TPA injected (red area, n=6, mean ± s.d.) mice were negative and positive inflammatory control. Significant difference (** p<0.01) between positive inflammatory control and negative inflammatory control as well as all injected hydrogels (n=8-10, mean + s.d.) could be observed. No significant difference in lymph node size between negative control and injected hydrogels was detected. (**b**) Anatomical proximity of inguinal lymph nodes and injected

hydrogels is shown. (**c**) MRI images of hydrogel injected, untreated (negative control), and TPA injected mice are shown. Inguinal lymph nodes (red circles with arrow) and injected hydrogels (red arrows) are within the same anatomical area. (**d**) IL-6 and (**e**) TNF-α levels of serum samples (n=3 animals, mean + s.d.) measured by ELISA are shown. Dotted line and green area represent untreated, dotted line and red area TPA treated control animals (n=3 animals, mean ± s.d.).
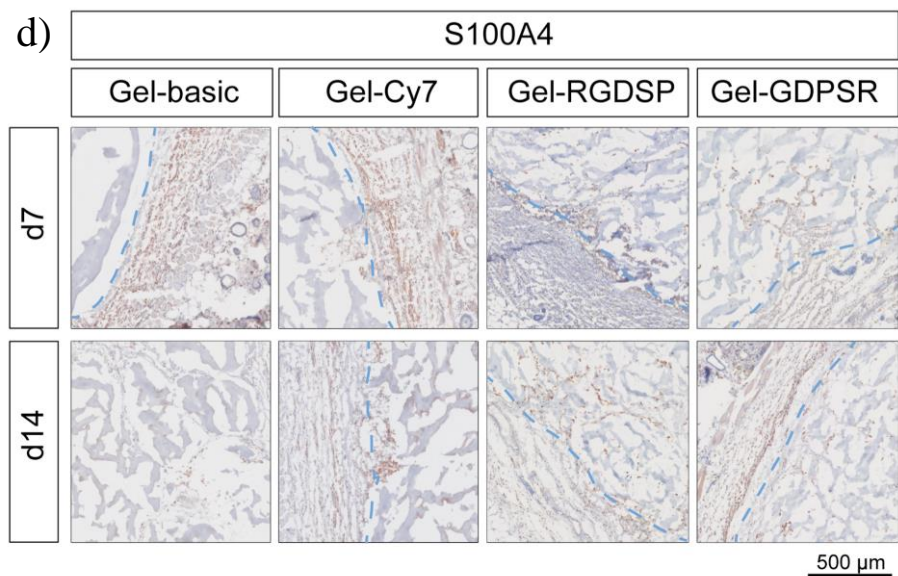
a) CD68

Gel-basic | Gel-Cy7 | Gel-RGDSP | Gel-GDPSR

d7

d14

500 µm

b) CD206

Gel-basic | Gel-Cy7 | Gel-RGDSP | Gel-GDPSR

d7

d14

500 µm

c) CD31

Gel-basic | Gel-Cy7 | Gel-RGDSP | Gel-GDPSR

d7

d14

500 µm

Figure 5. Representative immunohistological images of (**a**) the pan-macrophage marker CD68, (**b**) the M2-macrophage marker CD206, (**c**) the blood vessel marker CD31, and (**d**) the fibroblast marker S100A4 7 days and 14 days after hydrogel injection. Cell nuclei in blue and positive immunohistological staining in red. Hydrogels were also stained in light blue due to the Hematoxylin. The blue dashed line indicates the hydrogel-tissue-interface.
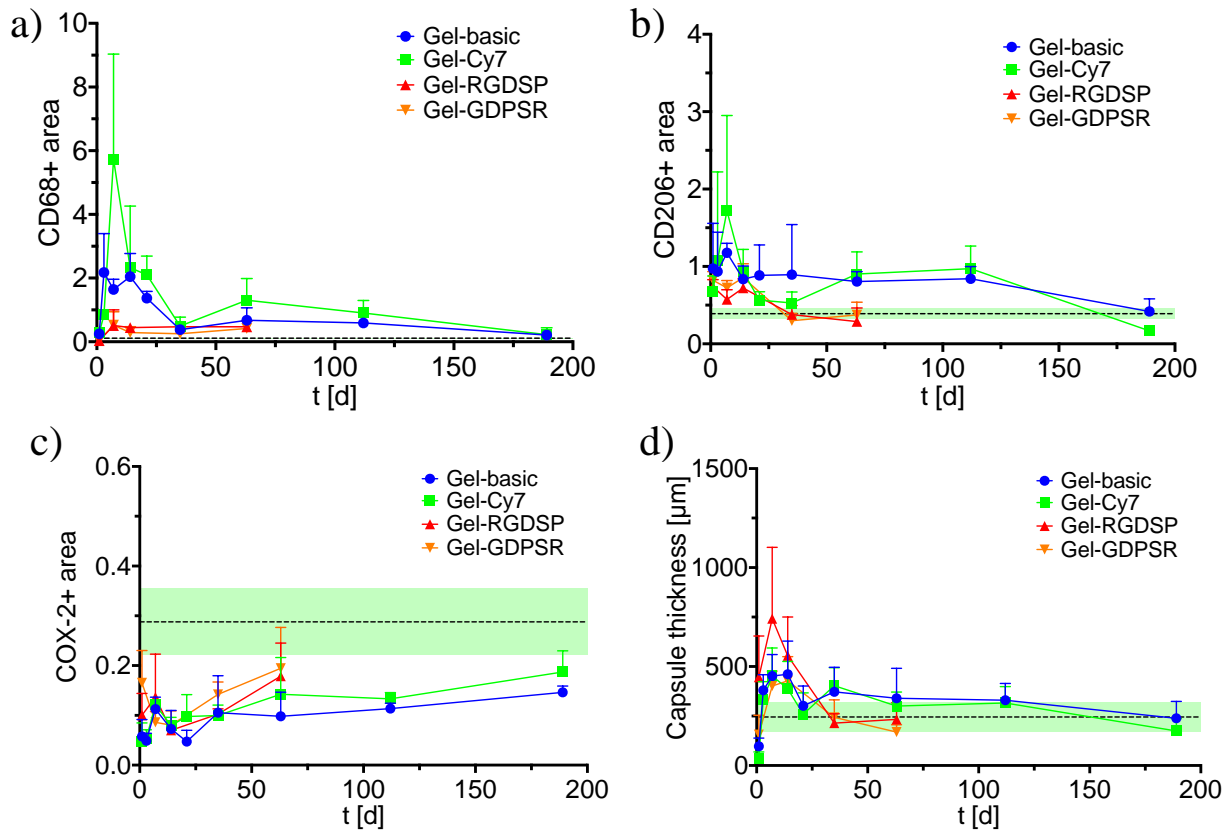
Figure 6. Immunohistological quantification of positive stained area compared to counterstaining of cell nuclei of hydrogel-injected animals. Course of time shown for (**a**) pan-macrophage marker CD68, (**b**) M2-macrophage marker CD206, and (**c**) COX-2 (n=3 different animals, mean + s.d.). Quantification was applied using color thresholds at mosaic images of whole, centric 10 µm slices of the hydrogel and the surrounding tissue. Dotted line and green area show the quantification for the untreated negative control animals (n=3 animals, mean ± s.d.). (**d**) Capsule thickness measured at van Gieson's staining around the hydrogel (n=3 different animals, 5 measuring points per implant site (skin or muscle) and per animal). Dotted line and green area show measurement for the untreated negative control animals (n=3 animals, mean ± s.d.).

Table 1. Antibodies used for immunohistological staining.

Antibody	Catalog no.	Dilution	Species	Antigen retrieval	Cell or tissue type
Primary antibody					
CD31 (abcam)	ab28364	1:75	Rabbit	Citrate buffer	Blood vessels[43]
CD68 (AbD Serotec)	MCA-1957	1:100	Rat	-	Macrophages[44]
CD206 (abcam)	ab64693	1:100	Rabbit	Citrate buffer	M2-macrophages[44]
COX-2 (abcam)	(ab15191)	1.500	Rabbit	Citrate buffer	Cyclooxygenase-2
Ki67 (abcam)	ab15580	1:200	Rabbit	Citrate buffer	Proliferatory cells[45]
S100A4 (Thermo Scientific)	RB-9411	1:100	Rabbit	Citrate buffer	Fibroblasts[46]
Isotype-control					
Rabbit polyclonal IgG (abcam)	ab27478	Concentration equal to primary antibody	Rabbit	Equal to primary antibody	
Normal rat IgG (Santa Cruz)	sc-2026	Concentration equal to primary antibody	Rat	Equal to primary antibody	
Secondary antibody					
Goat anti-rabbit (Dianova)	111-065-003	1:200	Goat		
Rabbit anti-rat (Dianova)	312-066-045	1:100	Rabbit		

A hydrogel system crosslinked by peptide-oligosaccharide non-covalent interaction exhibits fast self-healing and injectability. Injected hydrogels in immunocompetent mice and release of encapsulated compound were monitored up to 9 months by magnetic resonance imaging and optical imaging. This surprisingly stable hydrogel did not cause adverse inflammatory response, while its degradation is associated with invasion of macrophages and vascular formation.

Keyword
injectable hydrogels

Christoph Tondera, Robert Wieduwild, Elisabeth Röder, Carsten Werner, Yixin Zhang, Jens Pietzsch

High in vivo Biocompatibility of an Injectable Non-covalent Hydrogel System

(55 mm broad × 50 mm high)